The origin of the boson peak and thermal conductivity plateau in low-temperature glasses

Vassiliy Lubchenko and Peter G. Wolynes†

Department of Chemistry and Biochemistry, University of California at San Diego, La Jolla, CA 92093

Contributed by Peter G. Wolynes, December 21, 2002

We argue that the intrinsic glassy degrees of freedom in amorphous solids giving rise to the thermal conductivity plateau and the ''boson peak'' in the heat capacity at moderately low temperatures are directly connected to those motions giving rise to the two-level-like excitations seen at still lower temperatures. These degrees of freedom can be thought of as strongly anharmonic transitions between the local minima of the glassy energy landscape that are accompanied by ripplon-like domain wall motions of the glassy mosaic structure predicted to occur at T_g by the random first-order transition theory. The energy spectrum of the vibrations of the mosaic depends on the glass transition temperature, the Debye frequency, and the molecular length scale. The resulting spectrum reproduces the experimental low-temperature boson peak. The ''nonuniversality'' of the thermal conductivity plateau depends on $k_B T_g/\hbar\omega_D$ and arises from calculable interactions with the phonons.

A multitude of phenomena are observed in all low-temperature glasses that can only be explained by the existence of excitations not present in crystals. At very low temperatures, the universal scalings of heat capacity and thermal conductivity suggest these excitations cannot be simply ascribed to the local molecular motions specific to each substance (1–3). Yet quantitative analysis of the experiments has generally relied on purely phenomenological models that invoke unrelated types of excitations in different temperature regimes. At liquid helium temperatures, the excitations of glasses are well described as two-level systems (TLS; refs. 4–6), but at somewhat higher temperatures, the more mysterious ''boson peak'' appears in the heat capacity, and the phonon mean-free path falls precipitously, as if new scatterers became active, leading to a plateau in the thermal conductivity. Several different ideas about these additional excitations have been explored, ranging from harmonic excitations of a disordered lattice (7) to anharmonic local modes of a ''soft potential'' with distributed parameters (8).

In contrast, here we suggest, by using simple arguments, that like the TLS (9), most of the quantum excitations in glasses in this temperature regime are intrinsic and essential relics of the nonequilibrium character of the glass after it is prepared. We show that quantized ''domain wall motions'' connected with the mosaic structure of glasses predicted by the random first-order transition theory of glasses (10, 11) can explain the boson peak and conductivity plateau.

The random first-order transition theory of the glass transition suggests there is a dynamical mosaic structure in classical supercooled liquids (10–12). This mosaic structure is directly manifested in the dynamical heterogeneity observed in supercooled liquids using single-molecule experiments (13) and nonlinear relaxation experiments (14). Below T_g, the mosaic is spatially defined by the molecular motions that were not arrested at T_g and is thus only dynamically detectable. We have shown that these same motions at liquid helium temperatures would be quantized and can be described by the two-state system phenomenology (9). This identification predicts the density of states arising from these motions and accounts for the previously unexplained universality of thermal conductivity in the liquid helium temperature regime. As the temperature is raised, however, the theory indicates these excitations should lose their strict two-level character. The predicted temperature of the crossover to multilevel behavior coincides with the temperature regime where further excitable modes have been needed to explain experiments. In this paper, we show explicitly how the number of extra excitable modes of the mosaic accounts nearly quantitatively for the data, thus removing the need to invoke additional mechanisms, although other contributions may well be present to some extent (see, for example, ref. 15 on the contribution of purely harmonic modes to the heat capacity of simulated a-SiO_2 at this temperature). The excitations in the boson peak, like the TLS, active at lower temperatures, turn out to be collective motions of many particles ($\approx$200) encompassing rearrangements of a typical domain frozen in at the glass transition. The multilevel behavior of these domains can be pictured as involving the concomitant excitation of the ''ripplon'' modes of the glassy mosaic along with the transition between local minimum energy configurations of a mosaic cell. The knowledge of the spatial extent of the domain walls, along with their mass and surface tension (9), allows us to estimate approximately the ripplon spectrum with no adjustable parameters.

PHYSICS

The TLS Regime

According to the random first-order transition theory of supercooled liquids (10, 11), metastable configurations begin to last locally longer than a few vibrations just below a dynamical transition temperature T_A. Below this transition, a glass-forming liquid samples exponentially many metastable configurations much higher in energy than those of the corresponding crystal, but which are long lived. Glassy dynamics is described by the activated motions between minima. The liquid can be visualized as a mosaic of domains that locally resemble low-free-energy configurations that are separated from each other by frustrated higher energy interfaces, or domain walls. The length scale of the mosaic and number density of these walls is determined by the competition between the energy cost of a wall and the entropic advantage of using the large number of configurations. As temperature is lowered, the configurational entropy per particle, s_c, decreases so that the cooperative length grows. This leads to a larger activation barrier that eventually gives relaxation times exceeding the laboratory time scale. The size and rate of motion of these mosaic domains can be calculated without adjustable parameters once the liquid's heat capacity jump at the glass transition is known (12). In the classical regime, this theory leads to predictions of the average barrier and distributions of barriers in quantitative agreement with experiment (16). According to this microscopic calculation, at the T_g that corresponds with 1 hour relaxation time, the size of the cooperative region ξ in terms of the molecular length scale a is expected to vary only a little from substance to substance. A mosaic cell allows for at least one alternative kinetically accessible configuration at T_g. These alternate states, therefore, have spectral density $\approx 1/T_g$ per domain of size ξ^3 (9). This value agrees with the measured

Abbreviation: TLS, two-level systems.

†To whom correspondence should be addressed. E-mail: pwolynes@chem.ucsd.edu.

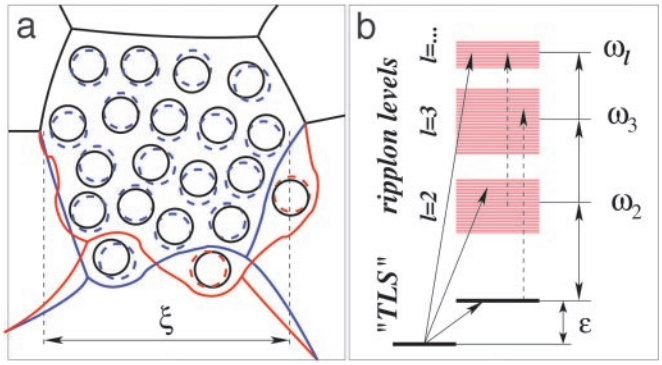

Fig. 1. (*a*) Schematic of a tunneling mosaic cell, with doubled circles denoting atomic tunneling displacements. The boundary's location is variable, as illustrated (in an exaggerated manner) by the blue and red lines. The domain wall distortion amounts to populating ripplon states on top of the structural transition energy ε, as shown in *b*. All transitions exemplified by solid lines involve tunneling between the intrinsic states. Those transitions are coupled linearly to the lattice distortion and contribute the strongest to the phonon scattering. The ''vertical'' transitions, denoted by the dashed line, are coupled to the higher order strain; they contribute only to the Rayleigh scattering (which is too weak to account for the plateau; ref. 17).

density of TLS (6). Although they are activated at T_g, at temperatures below T_g, motions between these alternative states remain possible, switching to coherent resonant tunneling at a temperature proportional to but smaller than the Debye temperature: $\sim(a/\xi)T_D/2\pi$ (9).

The Boson Peak Regime of the Heat Capacity

At low temperatures, the TLS excitations involve tunneling of the mosaic cells typically containing $N^* \simeq 200$ atoms. The tunneling path involves stagewise motion of the wall separating the distinct alternative configurations through the cell until a near-resonant state is found. In this paper, we focus on the excitations at energies just *above* those typical of the TLS regime. At the corresponding temperatures, other final tunneling states are possible, because the exact number and identity of the atoms that tunnel can vary (see Fig. 1*a*). These new configurations typically will be like the near-resonant level but will also move a few atoms at the boundary, i.e., at the interface to another domain. These fluctuations of the domain boundary shape can be visualized as domain wall surface modes (ripplons). They cost a surface energy that varies with the size of the domain and have kinetic energy consistent with the mass of the moving domain wall. It is not surprising that the ripplon's frequencies turn out to be proportional to ω_D, the basic quantum energy scale in the system, just as the crossover temperature does. A detailed calculation of the ripplon spectrum would require a considerable knowledge of the topology and statistics of the mosaic. At each temperature below T_A, the domain wall foam is an equilibrium structure made up of nearly flat patches. According to the random first-order transition theory, the effective surface tension depends on the curvature and vanishes at large radius of curvature as $\sigma(r) \propto r^{-1/2}$. To approximate the spectrum, we notice that the ripples of wave-length larger than the size of a patch will typically sense a roughly spherical surface of radius $R = \xi(3/4\pi)^{1/3}$. The surface tension of the mosaic has been calculated from the classical microscopic theory and is given by $\sigma(R) = \frac{3}{4}(k_BT_g/a^2)\log((a/d_L)^2/\pi e)(a/R)^{1/2}$ (12), where d_L/a is the universal Lindemann ratio of the vibrational amplitude at the glass transition to the molecular length scale. By itself, such a tension would collapse the mosaic, but this tension should be compensated for by stretching the frozen-in outside walls of neighboring mosaic cells. This compensating effect can be approximated by an isotropic positive pressure of a ghost (i.e., vanishing density) gas on the inside. Calculating the frequencies of the surface eigen-modes of a hollow sphere, subject to surface tension, is a classic problem of mathematical physics (18). Accounting for the unusual r dependence of the surface tension $\sigma(r) \propto r^{-1/2}$ modifies the standard result for the frequencies by a factor of 9/8. The eigen modes have frequencies $\omega_l^2 = \frac{9}{8}(\sigma/\tilde{m}_W R^2)(l-1)(l+2)$, where $\tilde{m}_W = (d_L/a)^2\rho a$ is the domain wall mass per unit area (9) and ρ is the mass density of the glass. The l-th mode of a sphere is $(2l+1)$-fold degenerate. By using $k_BT_g \simeq \rho c_s^2 a^3 (d_L/a)^2$ (9), one then finds $\omega_l \simeq 1.34\omega_D(a/\xi)^{5/4}\sqrt{(l-1)(l+2)/4} \simeq 0.15\omega_D\sqrt{(l-1)(l+2)/4}$. Because of the universality of the (a/ξ) ratio (12), ω_l is a multiple of the Debye frequency. Because of the material's discreteness, there are no harmonics of higher than 9th to 10th order, corresponding to an atomic scale half-wavelength. The lowest allowed ripplon mode is $l = 2$, and it has a frequency of $\sim$1 THz for silica. This value is in agreement with the boson peak in the inelastic neutron scattering data (19). $l = 1$ corresponds to a domain translation and is accounted for by the underlying phonon momentum nonconserving tunneling transition itself. The $l = 0$ is a uniform domain dilation relevant to aging below T_g. The existence of the domain wall vibrations lets us visualize the multilevel character of the tunneling centers as exhibited at temperatures above the TLS regime. A schematic of the resultant droplet quantized energy levels is shown in Fig. 1*b*.

The (classical) density of energy minima of a domain is

$$n(\varepsilon) = \frac{1}{k_BT_g}e^{\varepsilon/k_BT_g}$$

(9), where the energy zero corresponds to the (high-energy) configuration frozen-in at T_g. The negative ε's correspond to some of the very numerous but mostly unavailable lower lying energy states that are accessed by tunneling. With the lower state of the resonant pair taken as the local ground state, the TLS spectral density becomes

$$n(\varepsilon) = \frac{1}{k_BT_g}e^{-|\varepsilon|/k_BT_g}.$$

The partition function of a domain with an excitation energy ε, possibly accompanied by populating vibrational states on top, is given by $Z_\varepsilon = 1 + e^{-\beta\varepsilon}\prod_l Z_l^{2l+1}$, where $Z_l \equiv 1/(1-e^{-\beta\hbar\omega_l})$ is the partition function of an l-th order ripplon mode. Apart from the excitation ε, we assume here that each ripplon has a nearly harmonic spectrum. Note that our energy level scheme automatically insures that the atomic motions near the thermally inactive defects will only contribute to the regular lattice vibrations. The specific heat per domain, calculated from Z_ε and averaged over $n(\varepsilon)$, is shown in Fig. 2.

The Thermal Conductivity Plateau

To estimate the scattering by the domain tunneling accompanied by the ripplons and thus the heat conductivity, we need to know the effective *scattering* density of states, the transition amplitudes, and the coupling to the phonons. Any transition in the domain accompanied by a change in its internal state is coupled to the gradient of the elastic field with energy $g \sim \rho c_s^2 \int d\mathbf{s}\cdot\mathbf{d}(\mathbf{r})$, where $\mathbf{d}(\mathbf{r})$ is the molecular displacement at the droplet edge because of the transition (9). Therefore, any transitions between groups marked with solid lines in Fig. 1*b* are coupled to the phonons with the same strength as the underlying (TLS-like) transition, shown to be $g \simeq \sqrt{k_BT_g\rho c_s^2 a^3}$ (9), and no selection rules apply for the change in the ripplon quantum numbers because of the strong anharmonicity. We do not possess detailed information on the transition amplitudes; however, they should be on the order of the transition frequencies themselves, just as

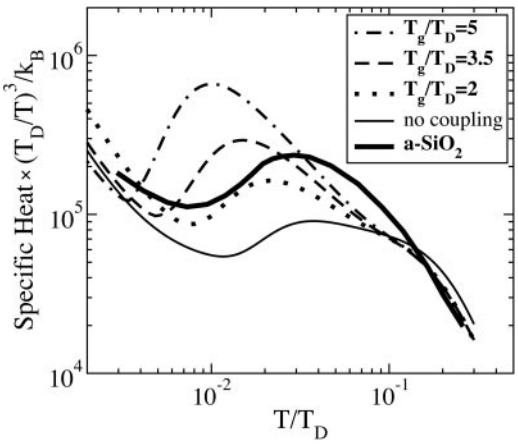

Fig. 2. The heat capacity per domain, which follows from the derived TLS + ripplon density of states, divided by T^3. This includes the Debye contribution. The thin line neglects phonon coupling and has $T_g/T_D = 4$. The experimental curve for amorphous silica from ref. 20, originally given in J/gK^4, is shown multiplied by $\hbar^3\rho c_s^3(6\pi^2)(\xi/a)^3/k_B^4$, where we used $\omega_D = (c_s/a)(6\pi^2)^{1/3}$, $(\xi/a)^3 = 200$ (9), $\rho = 2.2$ g/cm^3, $c_s = 4{,}100$ m/sec, and $T_D = 342$ K (3). By using the appropriate value of $k_BT_g/\hbar\omega_D = 4.4$ for a-SiO$_2$ would place the peak somewhat lower in temperature than observed.

for those TLSs that are primarily responsible for the phonon absorption at the lower T whose transition amplitudes are also comparable to the total energy splitting.

Because all transitions couple equally to the phonons, we can now calculate the density of the scattering states. The phonon-absorbing transition may occur from the ground state. The corresponding total number of ways to absorb a phonon of energy $\hbar\omega$ is $\rho(\omega) = \int_0^\infty d\varepsilon\ n(\varepsilon)\Sigma_{\{n_{lm}\}}\ \delta(\hbar\omega - [\varepsilon + \Sigma_{lm}n_{lm}\hbar\omega_{lm}]) = 1/k_BT_g\Sigma_{\{n_{lm}\}}\ \theta(\omega - \Sigma_{lm}n_{lm}\omega_{lm})e^{-\beta_g\hbar(\omega-\Sigma_{lm}n_{lm}\omega_{lm})}$, where we sum over all occupation numbers of the ripplons with quantum numbers l, m ($m = -l \ldots l$). The transition also may occur from the higher energy conformational state (thus $\varepsilon < 0$ in Fig. 1*b*), and we have to compute $\rho(\omega)$ from these states too. To find $\rho(\omega)$, we compute the cumulative density of states $N_E(\omega) \equiv \int_0^E d\varepsilon\ n(\varepsilon)\Sigma_{\{n_{lm}\}}\ \delta(\hbar\omega - [\Sigma_{lm}n_{lm}\hbar\omega_{lm} - \varepsilon])$. In a calculation parallel to obtaining Z_l, this quantity can be evaluated by using an integral representation of the step function θ along with the use of steepest descent. The scattering from excited states is proportional to $\rho_{exc}(\omega, T) \equiv \int_0^\infty dE\ f(E, T)\partial N_E(\omega)/\partial E$, where $f(E, T) \equiv 2/(e^{\beta\varepsilon} + 1)$ gives the appropriate Boltzmann weights.

Accurate calculation of the heat conductivity requires solving a kinetic equation for the phonons coupled with the multilevel systems, which would account for saturation effects, etc. Instead, we use a single relaxation time approximation for each phonon frequency. The Fermi golden rule yields for the scattering rate of a phonon with $\hbar\omega \sim k_BT$ the relation

$$\tau_\omega^{-1} \sim \omega\frac{\pi g^2}{\rho c_s^2}[\rho(\omega) + \rho_{exc}(\omega, T)].$$

The heat conductivity then equals $\kappa = \frac{1}{3}\Sigma_\omega\ l_{mfp}(\omega)C_\omega c_s$, where C_ω is the phonon heat capacity. At these energies, when the phonons are still relatively well defined ($l_{mfp}/\lambda > 1$), the heat has been shown to be carried primarily by phonons (21). The phonon mean free path will rapidly drop by the high T end of the plateau and will reach its minimum allowed value, which is the phonon's wave-length λ itself (the Ioffe–Riegel condition), as known empirically from ref. 3. To see how the conductivity depends on the temperature in this region, and thus account for multiple scattering/localization effects, we use the rough approximation $l_{mfp} = c_s\tau_\omega + \lambda$. At high T, the heat is not carried by "ballistic" phonons, but rather is transferred by a random walk from site to site, as originally anticipated by Einstein (22, 23) for homogeneous isotropic solids.

Damping Interaction with Phonons

The coupling of the multilevel excitations to phonons leads to significant frequency shifts and damping of the resonant transitions. To compute these coupling effects, we replace the discrete summation over the different uncoupled harmonics Σ_l $\int d\omega\ \delta(\omega - \omega_l)$ by integration over "Lorentzian" profiles

$$\sum_l\int d\omega\ \frac{\gamma_\omega/\pi}{[\omega-\omega_l(\omega)]^2+\gamma_\omega^2},$$

where γ_ω is a (frequency-dependent) friction coefficient, and $\omega_l(\omega)$ is the renormalized ripplon frequency, which has been shifted because of the corresponding dispersion effects. The total relaxation rate of a transition involving more than one mode is thus the sum of the inverse lifetimes of the participating modes. This assumption would be entirely correct for a frequency-independent γ, but should still be an adequate approximation at the low T end of the plateau, where the absorption is mostly caused by single ripplon mode processes. The mode decay rate γ_ω is the phonon irradiation-induced drag equal in the lowest order of perturbation to

$$\gamma_\omega = \frac{g^2}{4\pi\rho c_s^2}(\omega/c_s)^3 \simeq \frac{3\pi}{2\hbar}k_BT_g(\omega/\omega_D)^3,$$

where we do not distinguish between the longitudinal and transverse phonons. The corresponding (frequency-dependent) ripplon frequency shift required by the Kramers–Kronig relation gives a renormalized frequency

$$\omega_l(\omega) = \omega_l - \frac{3}{2\hbar}k_BT_g(\omega_c/\omega_D)^3f_0^{\omega_c}\frac{d\omega'(\omega'/\omega_c)^3}{\omega' - \omega},$$

where the principal value integral (numerically $\sim$1) is a slow (but sign-changing) function of ω and the cut-off frequency ω_c. ω_c is of the order (but greater than) $(a/\xi)\omega_D$, because the phonons

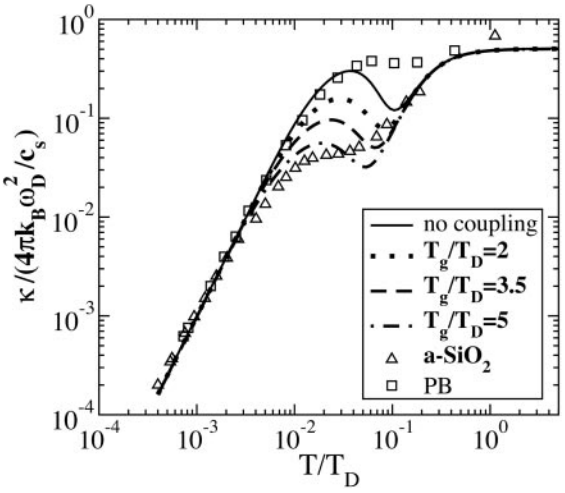

Fig. 3. The predicted low T heat conductivity. The "no coupling" case neglects phonon coupling effects on the ripplon spectrum. The (scaled) experimental data are taken from ref. 24 for a-Si ($k_BT_g/\hbar\omega_D \simeq 4.4$) and ref. 3 for polybutadiene ($k_BT_g/\hbar\omega_D \simeq 2.5$). The empirical universal lower T ratio $l_{mfp}/\lambda \simeq 150$ (3), used explicitly here to superimpose our results on the experiment, was predicted by the present theory earlier within a factor of order unity (9).

with wave-length shorter than ξ cause an increasingly smaller effective gradient of the phonon field as sensed by a region of size ξ. Although our approximation for γ_ω and $\omega_l(\omega)$ should break down in detail for $\omega > \omega_c$, it makes little difference computationally, as the damping is already very intense at this point. Both the frequency shift and the damping broaden the absorption peak, the former being quantitatively more important. Although the peaks' positions are determined by the quantum energy scale ω_D, the spectral *shifts* are proportional to T_g. The nonuniversality of the $k_B T_g/\hbar\omega_D$ ratio, which varies over the range of 2–5, thus yields a nonuniversal position of the plateau. This result is consistent with the experimentally observed material dependence in this regime. In Fig. 3, we show the resultant heat conductivities for different values of the ratio $k_B T_g/\hbar\omega_D$, using the specific cutoff $\omega_c = 1.8(a/\xi)\omega_D$. The nonmonotonic behavior exhibited by this approximation in the plateau region is likely an artifact of neglecting thermal saturation in the kinetic theory. Assuming that heat transport is dominated by thermal phonons alone leads to a temperature-independent $l_{mfp}(\omega)$ and a strictly horizontal plateau.

The coupling effects on the heat capacity can be obtained by replacing each Z_l with the formula for a damped oscillator. The resulting bump in c/T^3, shown in Fig. 2, is therefore also nonuniversal, depending on $k_B T_g/\hbar\omega_D$ being smaller for organic glasses, as seen in experiment.

We have concentrated here on the thermal phenomena ascribed to the boson peak in the glassy state itself at low temperature. Excitations of a similar frequency scale occur also above T_g and have been probed by various spectroscopies (e.g., see refs. 19 and 25). Although heavily damped, the existence of these excitations, analogous to those we discuss, on the basis of the random first-order transition theory is expected so long as the system is below T_A. These degrees of freedom doubtless coexist with other, more harmonic excitations at these frequencies. Separating their contributions to experiment requires detailed consideration of the coupling of the molecular motions to electromagnetic radiation or neutrons.

Conclusion

We have explained the microscopic origin of the excess of density of states in amorphous solids leading to the so-called boson peak in the heat capacity and a plateau in thermal conductivity. The dependence of the magnitude of those phenomena on the material constants, primarily T_g and ω_D, is given and is subject to experimental tests.

We thank Jörg Schmalian for reading and commenting on our manuscript. This work was supported by National Science Foundation Grant CHE-9530680.

1. Yu, C. C. & Leggett, A. J. (1988) *Comments Cond. Mat. Phys.* **14,** 231–251.
2. Leggett, A. J. (1991) *Physica B* **169,** 322–327.
3. Freeman, J. J. & Anderson, A. C. (1986) *Phys. Rev. B Solid State* **34,** 5684–5690.
4. Anderson, P. W., Halperin, B. I. & Varma, C. M. (1972) *Philos. Mag.* **25,** 1–9.
5. Phillips, W. A. (1972) *J. Low Temp. Phys.* **7,** 351–360.
6. Phillips, W. A., ed. (1981) *Amorphous Solids: Low-Temperature Properties* (Springer, Berlin).
7. Grigera, T. S., Martín-Mayor, V., Parisi, G. & Verrocchio, P. (2001) *Phys. Rev. Lett.* **87,** 085502.
8. Galperin, Y. M., Karpov, V. G. & Kozub, V. I. (1991) *Adv. Phys.* **38,** 669–737.
9. Lubchenko, V. & Wolynes, P. G. (2001) *Phys. Rev. Lett.* **87,** 195901.
10. Wolynes, P. G. (1992) *Acc. Chem. Res.* **25,** 513–519.
11. Kirkpatrick, T. R. & Thirumalai, D. (1995) *Transp. Theor. Stat. Phys.* **24,** 927–945.
12. Xia, X. & Wolynes, P. G. (2000) *Proc. Natl. Acad. Sci. USA* **97,** 2990–2994.
13. Russell, E. V. & Israeloff, N. E. (2000) *Nature* **408,** 695–698.
14. Sillescu, H. J. (1999) *NonCryst. Solids* **243,** 81–108.
15. Horbach, J., Kob, W. & Binder, K. (1999) *J. Phys. Chem.* **103,** 4104–4108.
16. Xia, X. & Wolynes, P. G. (2001) *Phys. Rev. Lett.* **86,** 5526–5529.
17. Anderson, A. C. (1981) in *Amorphous Solids: Low-Temperature Properties*, ed. Phillips, W. A. (Springer, Berlin).
18. Morse, P. M. & Feshbach, H. (1953) *Methods of Theoretical Physics* (McGraw–Hill, New York), Vol. 2, p. 1469.
19. Wischnewski, A., Buchenau, U., Dianoux, A. J., Kamitakahara, W. A. & Zarestky, J. L. (1998) *Phys. Rev. B Solid State* **57,** 2663–2666.
20. Pohl, R. O. (1981) in *Amorphous Solids: Low-Temperature Properties*, ed. Phillips, W. A. (Springer, Berlin).
21. Zaitlin, M. P. & Anderson, A. C. (1975) *Phys. Rev. B Solid State* **12,** 4475–4492.
22. Einstein, A. (1911) *Ann. Phys.* **35,** 679–694.
23. Cahill, D. G., Watson, S. K. & Pohl, R. O. (1992) *Phys. Rev. B Solid State* **46,** 6131–6140.
24. Smith, T. L. (1974) Ph.D. thesis (Univ. of Illinois, Urbana–Champaign).
25. Sette, F., Krisch, M. H., Masciovecchio, C., Ruocco, G. & Monaco, G. (1998) *Nature* **280,** 1550–1555.